Review Revision 2 Draft: NOT for Redistribution

A Survey Of Asteroid Destinations Accessible To Human Exploration

Daniel R. Adamo[*]
Astrodynamics Consultant, Houston, TX 77059

Jon D. Giorgini[†]
Jet Propulsion Laboratory, California Institute of Technology, Pasadena, CA 91109-8099

Paul A. Abell[‡]
NASA Johnson Space Center, Astromaterials Research and Exploration Science, Houston, TX 77058

Rob R. Landis[§]
NASA Ames Research Center, Intelligent Systems Division, Moffett Field, CA 94035

The Flexible Path is one of several space exploration strategy options developed by the Review of U.S. Human Space Flight Plans Committee (HSFPC). Among proposed Flexible Path destinations are near-Earth objects (NEOs), asteroids and comets having perihelions less than 1.3 astronomical units (AU) and periods less than 200 years. Heliocentric orbit element criteria are documented identifying the NEO subset potentially accessible to human exploration capabilities. Under HSFPC auspices, these criteria were applied to the Jet Propulsion Laboratory's (JPL's) small-body database (SBDB) in June 2009. The 36 NEOs identified as potentially accessible by this process are cited. Techniques are related with which opportunities to visit these "Accessible 36" NEO destinations are obtained and assessed over the interval from 2020 through 2050. Results from 20 of these assessments are presented. With the number of cataloged NEOs expected to grow by more than an order of magnitude in the next 20 years, the number and frequency of human NEO exploration opportunities will likewise increase.

I. Nomenclature

$C3$	=	spacecraft geocentric Earth departure energy (equivalent to v_{HE}^2)
$C3_X$	=	maximum C3 launch vehicle capability for a spacecraft of minimum mass = 45.2 mT
I_{SP}	=	propulsive specific impulse
a	=	near-Earth object (NEO) heliocentric orbit semi-major axis
a_A	=	maximum heliocentric semi-major axis of a spacecraft Earth departure trajectory with energy $C3_X$
a_P	=	minimum heliocentric semi-major axis of a spacecraft Earth departure trajectory with energy $C3_X$
e	=	NEO heliocentric orbit eccentricity
e_A	=	eccentricity of a spacecraft heliocentric elliptical orbit with apses r_A x r_M
e_P	=	eccentricity of a spacecraft heliocentric elliptical orbit with apses r_M x r_P
i	=	NEO heliocentric orbit inclination on the epoch J2000.0 ecliptic plane
i_X	=	spacecraft maximum attainable i after $C3_X$ is depleted by Δv
p	=	NEO heliocentric orbit semi-latus rectum
r_A	=	aphelion distance of a spacecraft Earth departure trajectory with semi-major axis a_A
r_{EPO}	=	geocentric radius of a circular Earth parking orbit (EPO)

[*] Sole Proprietor, 4203 Moonlight Shadow Ct., adamod@earthlink.net, and AIAA Senior Member.
[†] Senior Analyst, MS 301-150, 4800 Oak Grove Dr., jon.d.giorgini@nasa.gov.
[‡] Planetary Scientist, Code KR, paul.a.abell@nasa.gov.
[§] Aerospace Engineer, Code TI, rob.r.landis@nasa.gov.

r_M = spacecraft mean heliocentric distance at Earth departure = 1 AU = 149,597,870.691 km [7]
r_{MIN} = nominal (best-estimate) NEO minimum geocentric distance during an encounter with Earth
r_P = perihelion distance of an Earth departure trajectory with semi-major axis a_P
v_E = spacecraft heliocentric speed in the ecliptic plane at Earth departure
v_{EI} = geocentric spacecraft return trajectory speed at 121.92 km height (approximate entry interface) above a spherical Earth of radius 6378.136 km[7]
v_{HE} = geocentric spacecraft asymptotic hyperbolic excess speed as Earth's gravitational sphere of influence is departed
v_M = heliocentric spacecraft orbit speed at r_M
v_{MIN} = NEO geocentric speed at the r_{MIN} encounter epoch
v_R = NEO heliocentric radial velocity component at heliocentric distance r_M
v_T = NEO heliocentric tangential velocity component at heliocentric distance r_M
ΔT = spacecraft round trip mission duration
Δv = heliocentric velocity difference magnitude between a NEO orbit crossing a circular orbit of radius r_M
Δv_A = NEO-relative spacecraft arrival speed
Δv_D = NEO-relative spacecraft departure speed
Δv_{TNI} = trans-NEO injection change-in-velocity magnitude required to depart a circular EPO of radius r_{EPO} and achieve v_{HE}
δ = NEO geocentric true declination
δ_D = spacecraft Earth departure hyperbolic escape asymptote true declination
δ_R = spacecraft Earth return hyperbolic approach asymptote true declination
μ = Sun's reduced mass = 132,712,439,940 km^3/s^2 [7]
μ_E = Earth's reduced mass = 398,600.440 km^3/s^2 [7]
ν = NEO heliocentric true anomaly when heliocentric distance is r_M

II. Introduction

During mid-2009, the Review of U.S. Human Space Flight Plans Committee (HSFPC) requested a survey of known asteroids be conducted with the objective of identifying near-Earth objects (NEOs) accessible to anticipated human exploration capabilities beyond low Earth orbit (LEO). This research into NEO accessibility is associated with the HSFPC's Flexible Path exploration strategy option [1]. The Flexible Path avoids transporting humans to any near-term exploration destination deep in an extraterrestrial gravity well, such as the surfaces of the Moon or Mars. Instead, human exploration destinations beyond LEO are initially limited to lunar orbit, libration points in the Earth/Moon or Sun/Earth systems, NEOs, and eventually Mars orbit. After beyond-LEO human transport technology and infrastructure have advanced sufficiently on the Flexible Path, capabilities to land on destinations such as the Moon and Mars are anticipated. Pending those milestones, NEOs will be the primary extraterrestrial surfaces with which humans will directly interact on the Flexible Path [2].

The HSFPC-motivated survey of known asteroids identifies accessible NEO destinations through a progressive sequence of stages as follows.

1) Filter the small-body database (SBDB) maintained by the Jet Propulsion Laboratory (JPL) based on heliocentric semi-major axis "a", eccentricity "e", and ecliptic inclination "i". Accessibility threshold values for these orbit elements are driven by optimistic launch vehicle performance assumptions intended to leave no viable NEO destination excluded. The SBDB filter assumes very close NEO approaches to Earth such that significant launch vehicle and spacecraft performance need not be budgeted in reducing outbound or return mission transit times to remain within mission duration limits associated with human accessibility. Because the SBDB filter is blind to mission duration, NEOs it identifies are to be considered only *potentially* accessible. They may approach Earth in a sufficiently cooperative manner to become human exploration destinations only on rare occasions, if ever.
2) Using JPL-maintained ephemerides, search the notional time interval from 2020 through 2050 for sufficiently close encounters between Earth and each NEO identified as potentially accessible by the Stage #1 SBDB filter. With beyond-LEO human mission duration limited to less than a year by foreseeable

technology**, each viable human mission to a NEO destination from 2020 through 2050 will fall in the timeframe of the corresponding encounter. In cases where the NEO of interest has a poorly defined orbit in the SBDB, sufficiently accurate encounter predictions may not be known as far in the future as 2050. The search interval for these NEOs is curtailed accordingly.

3) Assuming unperturbed (conic) heliocentric motion, design optimized round trip trajectories from Earth, loitering a minimum of 10 days at a NEO destination. Each mission is conducted in a timeframe identified by Stage #2 for a Stage #1 NEO. Accessibility assessments for each NEO mission opportunity are then based on associated trajectory design parameters. These parameters are geocentric hyperbolic excess speed at Earth departure v_{HE}, true declination of the Earth departure hyperbolic escape asymptote δ_D, NEO-relative arrival speed Δv_A, NEO-relative departure speed Δv_D, Earth return entry interface speed v_{EI}, true declination of the Earth return hyperbolic approach asymptote δ_R, and round trip mission duration ΔT.

These stages are further documented in subsequent sections, together with summaries of their results when applied to a June 2009 SBDB survey.

III. Stage #1: The Small-Body Database (SBDB) Filter

An initial criterion with which to filter the current SBDB is launch vehicle Earth escape performance. In obtaining this specification, the strategy is to *overestimate* ultimately achievable Earth departure propulsive performance such that some exploration destinations accepted by the Stage #1 filter as viable will ultimately be found marginally *inaccessible* by Stage #2 and/or Stage #3. This Stage #1 "error condition" is preferred to otherwise viable destinations being rejected by overly conservative filtering criteria. The following assumptions are key to launch vehicle performance estimates.

A) The mission profile entails a single Ares V launch into a minimal altitude Earth parking orbit (EPO). Nominal loiter time in this EPO prior to trans-NEO injection (TNI) and Earth Departure Stage (EDS) cryogenic propellant depletion is at most 3 orbits.

B) Post-TNI, EDS-injected spacecraft (payload) mass is 45,243 kg. This equates to a minimal capability crew exploration vehicle (CEV) with capacity to impart NEO arrival and NEO departure impulses totaling 3.0 km/s using storable hypergolic propellant with specific impulse (I_{SP}) of 314 s††. The assumed CEV crew module mass is 9506 kg ([4] Table 5-1, p. 228, PDF p. 234), and the CEV "wet" service module mass is scaled by a factor of 2.62 from its Exploration Systems Architecture Study baseline ([4], Table 5-2, p. 241, PDF p. 247) to a value of 35,737 kg, thereby achieving the imposed 3.0 km/s capability.

In the context of permissive filtering criteria based on optimistic propulsive performance, it should be noted the filter is not a substitute for detailed mission analysis applied to a specific NEO destination during a specific timeframe. In particular, the following disclaimers will apply to destinations deemed accessible by the Stage #1 filtration process.

1) None of the filter criteria deal with mission duration. In general, shorter transit times between the Earth and a NEO destination will require greater propulsive capability from both the launch vehicle and spacecraft. Consequently, a viable NEO destination according to the filter may prove to be inaccessible when actual trajectory designs are computed whose transit times comply with human mission duration limits.

2) None of the proposed filter criteria deal with launch vehicle performance losses imposed by EPO equatorial inclination requirements. In general, v_{HE} or EDS-injected payload mass will be reduced if EPO equatorial inclination cannot be designed near 28.5°. Although a NEO destination's i may be small, the mission

** This one-year maximum mission duration assumption is highly arguable from the standpoint of prolonged micro-gravity and radiation exposure risks to human health in deep space. Accurate assessment of these risks becomes all the more uncertain when attempts are made to project human spaceflight technology into the mid-21st century. Nevertheless, until more is known about potential destination-specific NEO hazards such as rapid/chaotic rotation and surface cohesion, the most practical NEO missions for human exploration will be those with the shortest durations.

†† To place this 3.0 km/s propulsive capability in historic perspective, consider Apollo Command Service Module specifications [3] relating to Service Propulsion System (SPS) capability: total mass = 30,332 kg, usable SPS propellant mass = 18,413 kg, and SPS I_{SP} = 314 s. Assuming no additional Lunar Module mass, the SPS is capable of generating impulses totaling 2.876 km/s.

trajectory's $|\delta_D|$ may be large because the NEO can attain large $|\delta|$ near Earth. Large $|\delta|$ NEO geometry is likely to arise because, as observed in Disclaimer #1, close Earth approaches are compatible with sufficiently short human mission transits. The lowest possible EPO inclination supporting a coplanar TNI is equivalent to $|\delta_D|$ ([5], Figure 6.17).

Because Ares V is far from operational, the relationship between EDS-injected payload mass and C3 or v_{HE} is subject to appreciable revision. The Figure 1 plot ([6], p. 26) is used to obtain $C3_X = +11.1$ km^2/s^2 (equivalent to $v_{HE} = 3.33$ km/s) for a minimal 45.2 mT payload mass delivered to TNI from EPO equatorial inclinations near 28.5°. In personal communications with [6]'s author during mid-2009, Figure 1's pedigree has been verified to be highly optimistic in the context of initial human exploration capability beyond LEO. It exceeds current Ares V dispersed performance expectations by at least 10%.

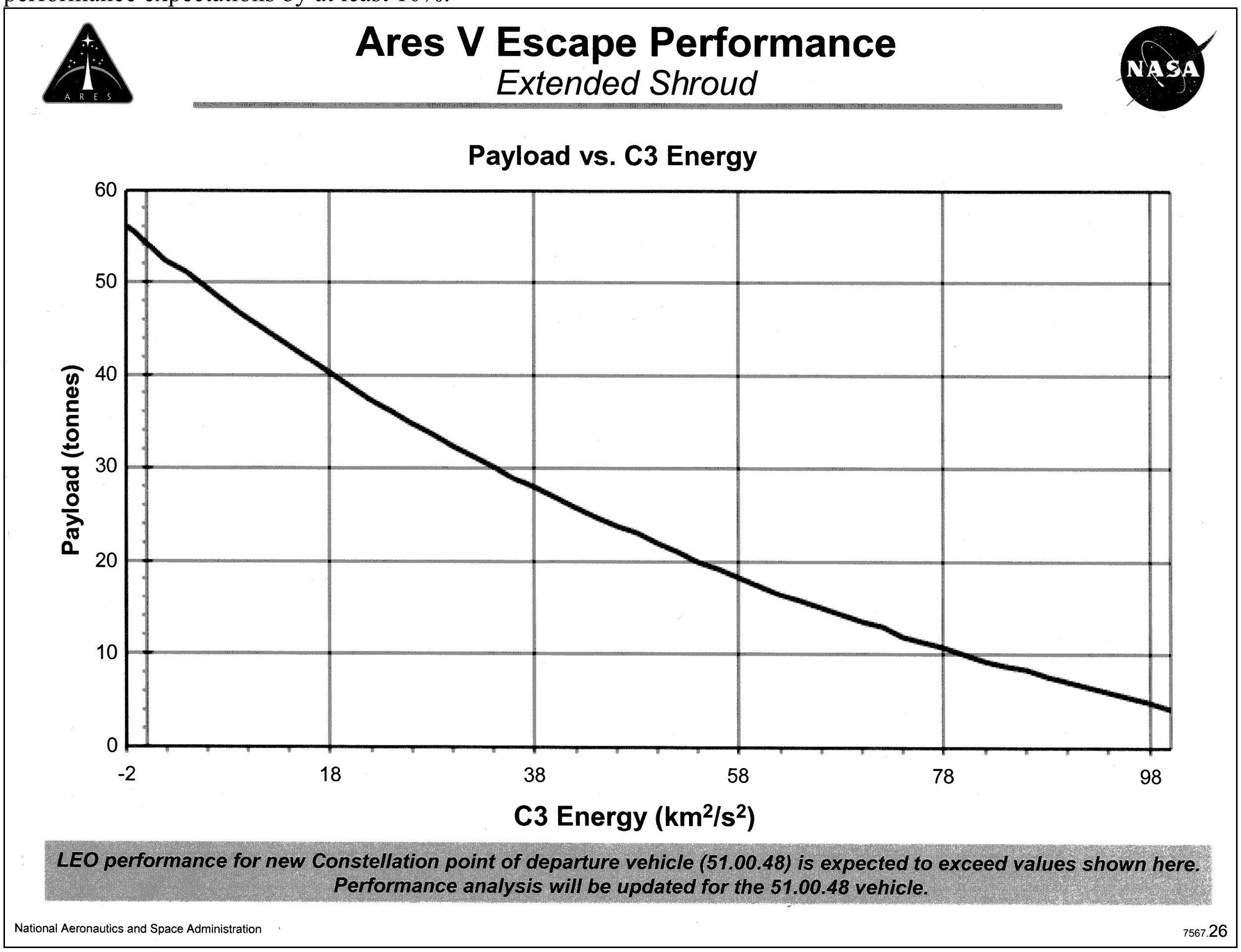

Figure 1: Ares V EDS-Injected Payload Mass Versus Earth Departure Energy ([6], p. 26)

The $C3_X$ capability initially defines an annular region in the ecliptic plane whose mean heliocentric radius‡‡ r_M is 1 AU. Circular orbit speed at r_M is v_M.

$$v_M = \sqrt{\frac{\mu}{r_M}} = 29.784692 \text{ km/s}$$

The annulus inner radius r_P is computed assuming $C3_X$ is applied as a retrograde Earth departure impulse.

$$a_P = \left[\frac{2}{r_M} - \frac{\left(v_M - \sqrt{C3_X}\right)^2}{\mu} \right]^{-1} = 123{,}511{,}664 \text{ km} = 0.825624 \text{ AU}$$

‡‡ This mean radius is not geometric because annulus inner and outer radii are reckoned by nonlinear heliocentric energy deviations about the mean radius value.

$r_P = 2\, a_P - r_M = 97{,}425{,}458$ km = 0.651249 AU

Similarly, the annulus outer radius r_A is computed assuming $C3_X$ is applied as a posigrade Earth departure impulse.

$$a_A = \left[\frac{2}{r_M} - \frac{\left(v_M + \sqrt{C3_X}\right)^2}{\mu} \right]^{-1} = 195{,}867{,}433 \text{ km} = 1.309293 \text{ AU}$$

$r_A = 2\, a_A - r_M = 242{,}136{,}996$ km = 1.618586 AU

A heliocentric elliptical orbit with apses r_M x r_P will have eccentricity e_P, and a complementary orbit in the annulus with apses r_A x r_M will have eccentricity e_A.

$$e_P = \frac{r_M}{a_P} - 1 = 0.211204$$

$$e_A = \frac{r_A}{a_A} - 1 = 0.236229$$

Now consider a NEO orbit with cataloged heliocentric semi-major axis "a" and eccentricity "e". Effective Earth/NEO heliocentric velocity difference magnitude Δv is to be computed by assuming a close approach between the two orbits facilitating sufficiently short human mission transit times. This process begins by determining the NEO orbit's semi-latus rectum.

$$p = a\,(1 - e^2) \tag{1}$$

The polar equation for conic sections then leads to trigonometric expressions for true anomaly ν when the NEO's heliocentric distance is r_M. For purposes of Δv computation, ν is confined to quadrants 1 and 2.

$$\cos\nu = \frac{\frac{p}{r_M} - 1}{e} \tag{2}$$

$$\sin\nu = \sqrt{1 - \cos^2\nu} \tag{3}$$

The component of NEO heliocentric radial velocity at heliocentric distance r_M arises from the time derivative of the polar equation for conic sections.

$$v_R = \sqrt{\frac{\mu}{p}}\, e \sin\nu \tag{4}$$

The component of NEO heliocentric tangential velocity at heliocentric distance r_M arises from the time derivative of the scalar relationship between ν and angular momentum.

$$v_T = \sqrt{\frac{\mu}{p}}\,\left(1 + e\cos\nu\right) \tag{5}$$

Spacecraft heliocentric speed in the ecliptic plane at Earth departure is determined by the foregoing components.

$$v_E = \sqrt{v_R^2 + v_T^2} \tag{6}$$

Assuming Earth's heliocentric orbit is circular with radius r_M, Δv can then be computed.

$$\Delta v = \sqrt{v_R^2 + \left(v_T - v_M\right)^2} \tag{7}$$

In cases where $|\cos\nu| > 1$ in Equation 2, r_M is not intermediate to the NEO orbit's apses. For these instances, "e" is ignored, Equation 6a replaces Equation 6, and Equation 7a replaces Equation 7.

$$v_E = \sqrt{\mu\left(\frac{2}{r_M} - \frac{1}{a}\right)} \tag{6a}$$

$$\Delta v = |\, v_E - v_M \,| \tag{7a}$$

The residual $C3_X - \Delta v^2$ approximates surplus launch energy available to attain the NEO orbit plane. Assuming this residual is positive, the maximum attainable heliocentric inclination i_X can be estimated.

$$i_X = \arctan\left(\frac{\sqrt{C3_X - \Delta v^2}}{v_E}\right) \tag{8}$$

With this formulaic background documented, filter processing and logic is summarized using the following procedural steps.

1) Specific to a NEO destination candidate being filtered, fetch heliocentric semi-major axis "a", eccentricity "e", and ecliptic inclination "i" from JPL's SBDB. Proceed to Step #2.

2) If $a_P < a < a_A$, proceed to Step #3. Otherwise, this NEO is rejected and Step #1 may be performed for another candidate.
3) If ($a < r_M$ and $e < e_P$) or if ($a \geq r_M$ and $e < e_A$), proceed to Step #4. Otherwise, this NEO is rejected and Step #1 may be performed for another candidate
4) Compute p from Equation 1 and cos ν from Equation 2. If |cos ν| > 1, compute Δv from Equation 6a and Equation 7a. Otherwise, compute Δv with Equation 3 through Equation 7. Proceed to Step #5.
5) If $\Delta v^2 < C3_X$, proceed to Step #6. Otherwise, $i_X \equiv 0$, this NEO is rejected, and Step #1 may be performed for another candidate.
6) Compute i_X from Equation 8. If $i < i_X$, this NEO is accepted as a viable destination; otherwise it is rejected. Step #1 may be performed for another candidate.

Table 1 contains numeric filtering examples applied to current NEO element sets obtained from JPL's *Horizons* ephemeris system [7]. A red value is cause for rejection as a viable destination, while green signifies a passed criterion necessary for acceptance as a viable NEO destination. Thus, (2000 SG_{344}) and (1999 AO_{10}) are the only viable destinations in Table 1. Because i_X is a computed filter criterion, it has no Table 1 coloration and is included for comparison with i. In shaded Table 1 cases, where i_X = 0 per filter Step #5, it is then possible to assess i according to filter Step #6 and color its value accordingly. Given that Step #5 has already rejected a NEO with i_X = 0, assessing i in such cases is purely for reference purposes.

Table 1: SBDB Filtration Examples

Filter Quantity	(2000 SG_{344})	(1999 AO_{10})	(2003 YS_{70})	(433) Eros	(99942) Apophis	(25143) Itokawa	(4660) Nereus
a (AU)	0.982804	0.910773	1.317601	1.458252	0.922378	1.322775	1.488671
e	0.065447	0.112650	0.252754	0.222907	0.191055	0.279444	0.360147
i (deg)	0.108	2.263	0.403	10.829	3.331	1.728	1.433
Δv (km/s)	1.889514	2.207358	4.196370	4.360665	5.194682	5.604860	6.778057
i_X (deg)	5.310	5.041	0	0	0	0	0

In June 2009 [8], JPL used foregoing computations and logic to filter the current SBDB for viable destinations. The three dozen NEOs identified by this process have come to be known as the Accessible 36 and are summarized by Table 2 in order of decreasing diameter[§§].

Table 2: The Accessible 36 NEO Destinations In Order Of Decreasing Approximate Diameter

Designation	a (AU)	e	i (deg)	Approx. Dia. (m)
(1996 XB_{27})	1.188926	0.057895	2.465	150
(1998 HG_{49})[***]	1.201267	0.113052	4.195	143
(2001 BB_{16})	0.854315	0.172498	2.027	104
(2003 SM_{84})	1.125731	0.082259	2.795	99
(2000 AE_{205})	1.164083	0.137356	4.46	90
(2001 QJ_{142})	1.062293	0.086336	3.106	72
(1999 AO_{10})	0.911559	0.110971	2.622	57
(2008 BT_2)	1.173194	0.080773	3.075	47
(2008 CX_{118})	1.144725	0.035265	2.42	45
(2001 FR_{85})	0.982699	0.027874	5.244	43
(2000 SG_{344})	0.977455	0.066908	0.11	38
(2007 TF_{15})	1.107648	0.041611	4.185	34
(1999 CG_9)	1.060676	0.062472	5.158	31
(1993 HD)	1.126322	0.039145	0.552	30

[§§] Estimated NEO diameters appearing in Table 2 and throughout this paper are based on absolute magnitude and assume a geometric albedo of 0.15 [8]. They may be in error by a factor typically ranging from 0.5 to 2.

[***] Computation refinements to filter criteria since June 2009, as documented herein, find (1998 HG_{49}) Table 2 values produce i_X = 4.110°. Although (1998 HG_{49}) is rejected in accord with filter Step #6, it is retained as a viable human exploration destination throughout this paper because it was reported as such to the HSFPC. Its Stage #3 assessment also serves to illustrate mission design characteristics from targeting a marginally *inaccessible* NEO with respect to Stage #1 criteria.

Designation	a (AU)	e	i (deg)	Approx. Dia. (m)
(2005 ER_{95})	1.223111	0.15909	3.336	30
(2006 BZ_{147})	1.023436	0.098617	1.409	29
(2006 QQ_{56})	0.985266	0.045555	2.797	23
(2003 YN_{107})	0.989355	0.013997	4.32	19
(2006 UB_{17})	1.140651	0.103764	1.991	19
(2007 VU_{6})	0.976508	0.090496	1.223	17
(1999 VX_{25})	0.900003	0.139586	1.663	16
(2005 LC)	1.133458	0.102199	2.8	15
(2001 GP_{2})	1.037742	0.073962	1.279	14
(2005 QP_{87})	1.232859	0.17534	0.268	10
(2008 EA_{9})	1.059154	0.079842	0.424	10
(2006 JY_{26})	1.011314	0.083722	1.421	8
(2008 HU_{4})	1.096781	0.078187	1.322	8
(2008 KT)	1.015719	0.086706	1.991	8
(2009 BD)	1.008566	0.039071	0.382	8
(1991 VG)	1.026915	0.049141	1.446	7
(2007 UN_{12})	1.053823	0.060455	0.235	6
(2008 TS_{10})	1.257401	0.201616	1.459	6
(2000 LG_{6})	0.917411	0.111081	2.833	5
(2008 UA_{202})	1.033057	0.068465	0.264	5
(2006 RH_{120})	1.033211	0.024507	0.596	4
(2008 JL_{24})	1.038238	0.10663	0.55	4

IV. Stage #2: Destination NEO Encounters With Earth

As noted in Section III's SBDB filter Disclaimer #1, otherwise viable NEO destinations may never approach Earth closely enough to permit sufficiently short round trip mission duration $\Delta T < 365$ days. Section V documents experience with planning practical round trips to the Accessible 36. This experience indicates the NEO destination must approach Earth within ~0.1 AU as a necessary condition leading to sufficiently brief ΔT is . Because a NEO's encounter epoch with Earth falls in the timeframe of any practical mission, this epoch serves to initiate a more detailed Stage #3 mission design. A JPL *Horizons* search for Earth encounters within ~0.1 AU is performed for each Accessible 36 destination over the time interval from 2020 through 2050. Table 3 summarizes results from these searches, with encounters listed according to decreasing NEO diameter. It should be noted that any Table 3 encounter prediction could be affected by unknown systematic biases in the small number (<< 150) of astrometric measurements currently available for any of the referenced NEOs. Prediction uncertainty associated with any NEO destination would be improved by additional measurements, likely including ones by a robotic precursor spacecraft, well in advance of a human mission there.

Table 3: Earth Encounters With The Accessible 36 NEO Destinations

Encounter #	Designation	Approx. Diameter (m)	Cov. Abort Before 2051[†††]	Encounter Date	r_{MIN} (AU)	v_{MIN} (km/s)
1	(1996 XB_{27})	150	No	2027 Jul 29	0.156919	1.696
2	(1996 XB_{27})	150	No	2049 May 19	0.115122	0.852

[†††] This column indicates whether or not an encounter search by *Horizons* is aborted prior to the requested search interval's end on 2051 Jan 1. An abort is triggered when linearly propagated 3σ uncertainty in NEO position/velocity equates to an encounter epoch uncertainty exceeding ± 10 days. Consequently, a "Yes" in this column indicates reported encounters may be inaccurate (particularly in later years) and other encounters leading to possible mission opportunities from 2020 through 2050 may be missing altogether. A "No" indicates higher confidence in finding and reporting all Earth encounters pertaining to a specific NEO from 2020 through 2050. Even if encounter date uncertainty is less than ± 10 days, position uncertainty may extend over millions of km.

Encounter #	Designation	Approx. Diameter (m)	Cov. Abort Before 2051†††	Encounter Date	r_{MIN} (AU)	v_{MIN} (km/s)
3	(1998 HG_{49})	143	No	2031 Jul 27	0.163567	1.055
4	(2001 BB_{16})	104	No	2020 Mar 08	0.091314	6.489
5	(2001 BB_{16})	104	No	2035 Jan 06	0.037748	4.860
6	(2001 BB_{16})	104	No	2039 Mar 07	0.041600	4.698
7	(2003 SM_{84})	99	No	2040 Jul 26	0.063785	2.589
8	(2003 SM_{84})	99	No	2046 Jul 20	0.051413	1.503
9	(2000 AE_{205})	90	No	2048 Nov 28	0.068063	2.848
10	(2001 QJ_{142})	72	Yes	2024 May 09	0.059030	2.239
11	(1999 AO_{10})	57	No	2026 Feb 11	0.026794	2.679
12	(1999 AO_{10})	57	No	2045 Dec 26	0.076668	5.095
13	(2008 BT_{2})	47	Yes	2022 Mar 16	0.086192	1.547
14	(2008 CX_{118})	45	Yes	2024 Jul 18	0.090004	1.301
15	(2001 FR_{85})	43	No	2039 Mar 21	0.045029	3.162
16	(2001 FR_{85})	43	No	2039 Sep 28	0.030896	2.860
17	(2001 FR_{85})	43	No	2040 Mar 28	0.058253	3.179
18	(2001 FR_{85})	43	No	2040 Aug 14	0.096517	3.486
19	(2000 SG_{344})	38	Yes	2028 May 07	0.019622	2.034
20	(2000 SG_{344})	38	Yes	2029 Feb 16	0.052714	1.471
21	(2000 SG_{344})	38	Yes	2029 Jul 28	0.034215	1.189
22	(2000 SG_{344})	38	Yes	2029 Nov 21	0.045229	1.253
	(2007 TF_{15})	34	No			
23	(1999 CG_{9})	31	Yes	2034 Feb 6	0.045397	2.738
	(1993 HD)	30	Yes			
24	(2005 ER_{95})	30	Yes	2028 Mar 23	0.033469	2.636
25	(2006 BZ_{147})	29	No	2035 Feb 25	0.019218	3.897
26	(2006 BZ_{147})	29	No	2036 May 09	0.094208	3.083
27	(2006 BZ_{147})	29	No	2037 Aug 06	0.052206	2.041
28	(2006 BZ_{147})	29	No	2038 Aug 26	0.098697	6.195
29	(2006 QQ_{56})	23	No	2050 Apr 22	0.047459	1.579
30	(2006 QQ_{56})	23	No	2050 Aug 07	0.033290	1.666
	(2003 YN_{107})	19	No			
31	(2006 UB_{17})	19	Yes	2034 Oct 03	0.077556	3.772
32	(2007 VU_{6})	17	Yes	2034 Oct 06	0.032501	2.324
33	(1999 VX_{25})	16	Yes	2028 Sep 15	0.048372	4.497
34	(1999 VX_{25})	16	Yes	2034 Sep 28	0.026033	2.938
35	(2005 LC)	15	Yes	2040 May 30	0.030686	2.740
36	(2001 GP_{2})	14	Yes	2020 Oct 03	0.008029	2.486
37	(2001 GP_{2})	14	Yes	2048 Apr 19	0.089772	5.176
38	(2005 QP_{87})	10	No	2031 Sep 18	0.032880	3.533
39	(2008 EA_{9})	10	Yes	2020 Apr 25	0.074595	1.321
40	(2008 EA_{9})	10	Yes	2033 Nov 15	0.078024	3.695
	(2006 JY_{26})	8	No			
41	(2008 HU_{4})	8	Yes	2047 Jan 22	0.090688	1.437
	(2008 KT)	8	No			
42	(2009 BD)	8	Yes	2034 Mar 27	0.092508	3.703
43	(2009 BD)	8	Yes	2034 Sep 01	0.093932	1.598
44	(1991 VG)	7	No	2038 Nov 07	0.073178	3.052
45	(1991 VG)	7	No	2039 May 29	0.060540	1.483
46	(2007 UN_{12})	6	Yes	2020 Jul 04	0.043224	2.897
47	(2007 UN_{12})	6	Yes	2021 Jan 08	0.095489	2.013

Encounter #	Designation	Approx. Diameter (m)	Cov. Abort Before 2051†††	Encounter Date	r_{MIN} (AU)	v_{MIN} (km/s)
48	(2007 UN_{12})	6	Yes	2049 Apr 30	0.089922	1.770
49	(2008 TS_{10})	6	Yes	2032 Jul 31	0.092398	6.061
50	(2000 LG_6)	5	No	2036 Jun 24	0.026258	2.429
51	(2008 UA_{202})	5	Yes	2028 May 18	0.088711	4.943
52	(2008 UA_{202})	5	Yes	2029 Oct 20	0.013617	2.807
53	(2006 RH_{120})	4	Yes	2028 Aug 08	0.028815	0.215
54	(2006 RH_{120})	4	Yes	2044 Jun 07	0.064970	1.180
55	(2008 JL_{24})	4	No	2026 Mar 05	0.060990	2.403
56	(2008 JL_{24})	4	No	2026 Jun 21	0.093079	1.991
57	(2008 JL_{24})	4	No	2043 Dec 09	0.018955	3.319
58	(2008 JL_{24})	4	No	2045 May 17	0.016299	3.269

V. Stage #3: Destination NEO Human Mission Trajectory Design

In the context of human NEO exploration, viability of a Table 3 encounter must ultimately be assessed with a trajectory design in the corresponding timeframe. Such a design consists of an outbound leg departing Earth and arriving at the NEO destination 10 days or more before the return leg departs the NEO bound for Earth. Heliocentric conic arcs approximate both trajectory legs to sufficient accuracy. Therefore, Earth and NEO heliocentric positions at the termini of each trajectory leg are among the Lambert boundary conditions (LBCs) leading to trajectory solutions supporting mission viability assessment. Heliocentric NEO positions associated with these Lambert solutions are imported from JPL's *Horizons* ephemeris system, while those for Earth are computed via general perturbations theory [9]. To ensure reasonably brief transit times for each mission leg compatible with human endurance, LBCs are constrained such that only "short way" (Type I) trajectory solutions spanning less than a 180° heliocentric transfer angle are produced.

Pork chop charts (PCCs) are the primary aid in selecting notionally optimal departure and arrival dates for outbound and return trajectory legs. A PCC is an array of values, with each element corresponding to a unique Lambert heliocentric trajectory solution. Each column in a PCC array is dedicated to a departure date, and each row is dedicated to an arrival date. On the outbound trajectory leg, PCC arrays composed of v_{HE}, δ_D, or Δv_A values may be relevant. For the return trajectory leg, PCC arrays composed of Δv_D, v_{EI}, or δ_R values may be relevant. Values appearing in a PCC are arbitrarily color-coded to visually aid optimization. When populated by speed values, PCC elements greater than 5 km/s are colored red, and those less than 2.5 km/s are colored green. When populated by declination values, PCC elements whose magnitudes exceed 57° are colored red, and those whose magnitudes are less than 28.5° are colored green. Intermediate PCC values are pink in color. Notional optimization criteria are as follows in order of decreasing priority.

1) Following launch into an EPO of unknown geocentric radius r_{EPO}, three propulsive impulses are assumed for the mission. The TNI impulse Δv_{TNI} occurs in the EPO using relatively efficient cryogenic propellant. If r_{EPO} is known, Δv_{TNI} can be computed from a PCC's v_{HE} value as follows.

$$\Delta v_{TNI} = \sqrt{v_{HE}^2 + \frac{2\,\mu_E}{r_{EPO}}} - \sqrt{\frac{\mu_E}{r_{EPO}}}$$

The final two impulses occur at NEO arrival and departure (Earth return braking is assumed to be through atmospheric friction) using relatively inefficient, but storable, hypergolic propellant. Because of this inefficiency, Δv_A and Δv_D are to be minimized at the expense of v_{HE} as necessary. Effectively zero priority is given to minimizing v_{EI} because it has no propulsive cost‡‡‡.

2) As observed in Section III's SBDB filter Disclaimer #2, a geocentric Earth departure trajectory's asymptotic declination magnitude $|\delta_D|$ sets a lower limit on EPO equatorial inclination. Assuming a Florida launch into

‡‡‡ Heat shield thermal loads are relatable to v_{EI}, but Earth atmospheric entry shielding limits of future spacecraft are currently uncertain. The fastest v_{EI} experienced by humans was logged during Apollo 10 at 11.069 km/s ([10], p. 581).

a posigrade EPO, $|\delta_D| > 28.5°$ will impose a performance loss in achieving EPO. At $|\delta_D| > 57°$, additional launch performance losses are likely to be imposed by range safety constraints. Any of these losses will reduce the EDS propellant available to perform TNI for a given spacecraft payload mass at a given r_{EPO}. Consequently, $|\delta_D|$ will be minimized to the extent permitted by v_{HE}, Δv_A, and Δv_D. Effectively zero priority is given to minimizing $|\delta_R|$ because it imposes no propulsive cost.

3) Round trip mission duration ΔT is to be maintained at less than a year. This constraint addresses crew microgravity and radiation exposure concerns, but it may require considerable modification as means to mitigate these concerns are developed. Although a low-priority constraint in this list, sufficiently short ΔT is actually enforced by Stage #1's SBDB filter and by previously noted LBCs confining trajectory solutions to less than a 180° heliocentric transfer angle. Thus, missions with small v_{HE}, Δv_A, and Δv_D values naturally tend to possess sufficiently short ΔT values.

As an illustration of notionally optimized NEO human mission trajectory designs using data from Section IV, consider Table 3's Earth Encounter #11 with (1999 AO_{10}). Figures 2 through 5 are PCCs presenting v_{HE}, δ_D, Δv_A, and Δv_D values key to trajectory design in the Encounter #11 timeframe. Data circumscribed by boxes in these PCCs correspond to notionally optimal departure and arrival dates.

In arriving at notional dates from the ensuing PCC data, two conflicting trends must be resolved. The primary conflict arises between Δv_A, and Δv_D values in Figures 4 and 5, where minimal Δv_D in Figure 5 is obtained on (1999 AO_{10}) *departure* dates well before Figure 4's (1999 AO_{10}) *arrival* dates enjoying minimal Δv_A. Fortunately, a reasonable compromise between Δv_A and Δv_D trends can be achieved by selecting (1999 AO_{10}) arrival on 2026 Jan 7 with departure 10 days later. At the expense of greater mission duration ΔT, further Δv_A reduction could be achieved by selecting an earlier Earth departure date. Unfortunately, launch dates much earlier than 2025 Sep 19 lead to a second conflicting trend in Figure 3. Shifting Earth departure date earlier while maintaining (1999 AO_{10}) arrival on 2026 Jan 7 in Figure 3 rapidly increases δ_D, incurring significant launch performance losses and likely range safety constraint violations by late August 2026. The notional choice of outbound leg departure and arrival dates is fortunately supported by a reasonably small v_{HE} value in Figure 2.

◇	A	B	C	D	E	F	G	H	I	J	K	L
1	(1999 AO10)					Earth Depart Date						
2	Arrive Date	7/31/25	8/10/25	8/20/25	8/30/25	9/9/25	9/19/25	9/29/25	10/9/25	10/19/25	10/29/25	11/8/25
3	9/19/25	10.868	12.973	16.807	24.824	49.488						
4	9/29/25	7.620	8.639	10.389	13.511	20.101	40.337					
5	10/9/25	5.374	5.863	6.710	8.107	10.664	16.076	32.438				
6	10/19/25	3.789	4.007	4.427	5.097	6.264	8.425	12.840	26.154			
7	10/29/25	2.690	2.767	2.978	3.320	3.921	4.984	6.814	10.563	21.658		
8	11/8/25	1.984	1.987	2.097	2.288	2.646	3.263	4.223	5.896	9.189	18.799	
9	11/18/25	1.613	1.575	1.631	1.751	1.998	2.406	2.995	3.939	5.477	8.450	17.220
10	11/28/25	1.496	1.424	1.443	1.520	1.703	1.990	2.384	2.988	3.863	5.275	8.069
11	12/8/25	1.522	1.408	1.389	1.430	1.565	1.766	2.038	2.448	2.992	3.788	5.119
12	12/18/25	1.606	1.429	1.368	1.373	1.466	1.603	1.788	2.072	2.421	2.902	3.643
13	12/28/25	1.713	1.434	1.324	1.295	1.352	1.440	1.561	1.757	1.979	2.275	2.714
14	1/7/26	1.863	1.398	1.232	1.173	1.204	1.254	1.328	1.461	1.596	1.773	2.037
15	1/17/26	2.260	1.290	1.066	0.994	1.013	1.040	1.081	1.170	1.244	1.343	1.497
16	1/27/26	57.640	0.988	0.791	0.757	0.788	0.806	0.826	0.885	0.916	0.962	1.047
17	2/6/26	58.843	46.301	0.854	0.651	0.632	0.619	0.611	0.639	0.636	0.644	0.684
18	2/16/26	58.696	58.870	26.659	1.851	1.020	0.752	0.622	0.567	0.516	0.490	0.493
19	2/26/26	58.433	58.720	58.892	23.470	2.832	1.516	1.058	0.838	0.710	0.643	0.612
20	3/8/26	58.052	58.444	58.769	58.845	22.678	3.705	2.025	1.432	1.151	1.008	0.932
21	3/18/26	57.550	58.044	58.482	58.781	58.754	22.910	4.483	2.514	1.825	1.510	1.345
22	3/28/26	56.921	57.517	58.062	58.488	58.772	58.689	23.986	5.195	2.982	2.215	1.859
23	4/7/26	56.162	56.858	57.508	58.048	58.471	58.792	58.616	26.192	5.878	3.416	2.569

Figure 2: PCC With Geocentric Earth Departure Hyperbolic Excess Speed v_{HE} Values In km/s

◇	A	B	C	D	E	F	G	H	I	J	K	L
1	(1999 AO10)					Earth Depart Date						
2	Arrive Date	7/31/25	8/10/25	8/20/25	8/30/25	9/9/25	9/19/25	9/29/25	10/9/25	10/19/25	10/29/25	11/8/25
3	9/19/25	-12.431	-12.203	-11.817	-11.391	-11.041						
4	9/29/25	-11.075	-10.952	-10.649	-10.237	-9.800	-9.547					
5	10/9/25	-7.895	-7.861	-7.672	-7.334	-6.914	-6.690	-6.574				
6	10/19/25	-2.210	-2.253	-2.229	-2.030	-1.750	-1.787	-1.875	-2.033			
7	10/29/25	7.019	6.895	6.609	6.514	6.402	5.687	5.005	4.263	3.613		
8	11/8/25	20.762	20.539	19.592	18.804	17.722	15.613	13.780	11.928	10.298	9.345	
9	11/18/25	38.095	37.665	35.439	33.255	30.324	26.154	22.777	19.508	16.702	14.875	13.676
10	11/28/25	54.706	53.635	49.493	45.379	40.251	34.246	29.619	25.212	21.495	18.973	17.035
11	12/8/25	66.503	64.042	57.794	51.992	45.346	38.461	33.284	28.327	24.161	21.272	18.848
12	12/18/25	73.094	68.756	60.829	53.999	46.675	39.605	34.361	29.272	24.984	21.989	19.304
13	12/28/25	76.358	70.255	61.030	53.509	45.867	38.827	33.700	28.663	24.405	21.461	18.666
14	1/7/26	78.154	70.607	59.776	51.452	43.520	36.529	31.603	26.722	22.577	19.803	17.013
15	1/17/26	78.148	70.277	56.384	46.895	38.778	31.997	27.489	22.983	19.084	16.658	14.024
16	1/27/26	-2.880	64.335	43.388	34.004	27.549	22.165	18.950	15.573	12.295	10.614	8.474
17	2/6/26	-15.383	-52.871	-27.744	-11.113	-3.617	-2.256	-1.209	-1.012	-2.714	-2.706	-3.407
18	2/16/26	-16.466	-19.489	-75.385	-57.699	-47.673	-42.234	-37.595	-33.047	-33.077	-30.383	-28.074
19	2/26/26	-17.314	-19.827	-23.252	-80.766	-65.619	-62.523	-59.512	-56.077	-54.865	-49.481	-44.826
20	3/8/26	-18.084	-20.336	-22.704	-26.509	-85.203	-69.399	-65.601	-61.513	-57.536	-50.529	-44.591
21	3/18/26	-18.807	-20.864	-22.822	-24.961	-29.031	-89.412	-69.672	-63.942	-58.121	-50.326	-43.532
22	3/28/26	-19.491	-21.377	-23.069	-24.649	-26.450	-30.578	-85.401	-68.197	-60.574	-51.959	-44.221
23	4/7/26	-20.137	-21.862	-23.338	-24.584	-25.694	-27.056	-30.920	-80.194	-65.833	-55.827	-46.831

Figure 3: PCC With Geocentric Earth Departure Asymptotic Declination δ_D Values In deg

◇	A	B	C	D	E	F	G	H	I	J	K	L
1	(1999 AO10)					Earth Depart Date						
2	Arrive Date	7/31/25	8/10/25	8/20/25	8/30/25	9/9/25	9/19/25	9/29/25	10/9/25	10/19/25	10/29/25	11/8/25
3	9/19/25	20.273	22.827	26.927	35.043	59.549						
4	9/29/25	16.192	17.633	19.662	22.941	29.476	49.390					
5	10/9/25	13.042	13.894	14.988	16.546	19.092	24.258	40.191				
6	10/19/25	10.529	11.038	11.649	12.446	13.600	15.544	19.589	32.310			
7	10/29/25	8.496	8.791	9.129	9.545	10.100	10.946	12.436	15.653	26.076		
8	11/8/25	6.841	6.999	7.176	7.386	7.654	8.044	8.684	9.886	12.614	21.617	
9	11/18/25	5.494	5.564	5.644	5.741	5.866	6.051	6.355	6.902	7.997	10.520	18.826
10	11/28/25	4.401	4.416	4.442	4.481	4.538	4.633	4.800	5.099	5.664	6.779	9.282
11	12/8/25	3.523	3.507	3.509	3.526	3.561	3.626	3.743	3.947	4.308	4.944	6.126
12	12/18/25	2.832	2.804	2.806	2.828	2.868	2.935	3.044	3.217	3.490	3.920	4.615
13	12/28/25	2.317	2.288	2.312	2.357	2.419	2.504	2.620	2.781	3.008	3.325	3.785
14	1/7/26	1.983	1.951	2.017	2.097	2.184	2.285	2.406	2.554	2.743	2.984	3.302
15	1/17/26	1.922	1.794	1.919	2.029	2.130	2.233	2.344	2.470	2.620	2.796	3.014
16	1/27/26	56.161	1.852	2.042	2.145	2.228	2.308	2.392	2.484	2.588	2.706	2.844
17	2/6/26	57.459	45.980	2.685	2.507	2.481	2.495	2.525	2.567	2.620	2.680	2.749
18	2/16/26	57.315	57.468	27.159	3.650	2.998	2.814	2.739	2.707	2.696	2.694	2.699
19	2/26/26	57.206	57.481	57.616	24.097	4.510	3.430	3.084	2.916	2.815	2.740	2.678
20	3/8/26	57.117	57.513	57.798	57.882	23.369	5.233	3.777	3.277	3.015	2.838	2.698
21	3/18/26	57.037	57.556	57.969	58.259	58.265	23.643	5.830	4.037	3.387	3.028	2.778
22	3/28/26	56.956	57.598	58.137	58.566	58.860	58.778	24.790	6.334	4.209	3.411	2.959
23	4/7/26	56.860	57.626	58.293	58.853	59.298	59.598	59.448	27.130	6.779	4.298	3.354

Figure 4: PCC With (1999 AO_{10})-Relative Arrival Speed Δv_A Values In km/s

◇	A	B	C	D	E	F	G	H	I	J	K	L
1	Earth Return					(1999 AO10) Depart Date						
2	Date	11/28/25	12/8/25	12/18/25	12/28/25	1/7/26	1/17/26	1/27/26	2/6/26	2/16/26	2/26/26	3/8/26
3	12/3/25	31.575										
4	12/13/25	9.908	29.526									
5	12/23/25	5.500	9.016	26.785								
6	1/2/26	3.533	4.808	7.849	23.295							
7	1/12/26	2.366	2.920	3.957	6.458	19.189						
8	1/22/26	1.559	1.805	2.223	3.023	4.962	14.811					
9	2/1/26	0.972	1.077	1.256	1.573	2.185	3.653	11.015				
10	2/11/26	0.592	0.647	0.750	0.928	1.229	1.781	3.051	9.281			
11	2/21/26	0.555	0.615	0.718	0.875	1.109	1.475	2.117	3.577	10.768		
12	3/3/26	0.808	0.865	0.962	1.105	1.308	1.602	2.061	2.872	4.746	14.147	
13	3/13/26	1.142	1.178	1.257	1.377	1.548	1.788	2.139	2.691	3.680	6.018	17.875
14	3/23/26	1.497	1.496	1.543	1.633	1.767	1.956	2.225	2.621	3.249	4.409	7.194
15	4/2/26	1.870	1.810	1.813	1.862	1.954	2.093	2.291	2.575	2.998	3.696	5.016
16	4/12/26	2.285	2.131	2.072	2.073	2.118	2.205	2.340	2.537	2.826	3.279	4.056
17	4/22/26	2.788	2.479	2.332	2.271	2.263	2.298	2.375	2.501	2.692	2.997	3.506
18	5/2/26	3.500	2.894	2.609	2.464	2.394	2.374	2.396	2.462	2.579	2.785	3.143
19	5/12/26	4.798	3.471	2.936	2.670	2.523	2.443	2.411	2.423	2.482	2.620	2.889
20	5/22/26	8.636	4.500	3.388	2.911	2.657	2.508	2.421	2.383	2.395	2.485	2.701
21	6/1/26	48.638	7.391	4.185	3.243	2.815	2.574	2.426	2.341	2.314	2.371	2.558
22	6/11/26	61.227	39.182	6.378	3.832	3.036	2.654	2.432	2.299	2.239	2.274	2.448
23	6/21/26	61.186	60.270	31.151	5.460	3.434	2.770	2.442	2.255	2.165	2.187	2.360

Figure 5: PCC With (1999 AO_{10})-Relative Departure Speed Δv_D Values In km/s

To summarize, PCC data in Figures 2 through 5 facilitate a notionally optimized human mission trajectory design with major events appearing in Table 4.

Table 4: Major Events In A Notionally Optimized Human Mission To NEO (1999 AO_{10})

Date	Event
2025 Sep 19	Depart Earth: v_{HE} = 1.254 km/s, δ_D = +36.529°
2026 Jan 7	Arrive (1999 AO_{10}): Δv_A = 2.285 km/s
2026 Jan 17	Depart (1999 AO_{10}): Δv_D = 1.475 km/s
2026 Feb 21	Arrive Earth: v_{EI} = 11.332 km/s, δ_R = -9.570°, ΔT = 155 days

Outbound and return legs of the notionally optimized (1999 AO_{10}) trajectory are plotted heliocentrically in Figure 6 and geocentrically in Figure 7.

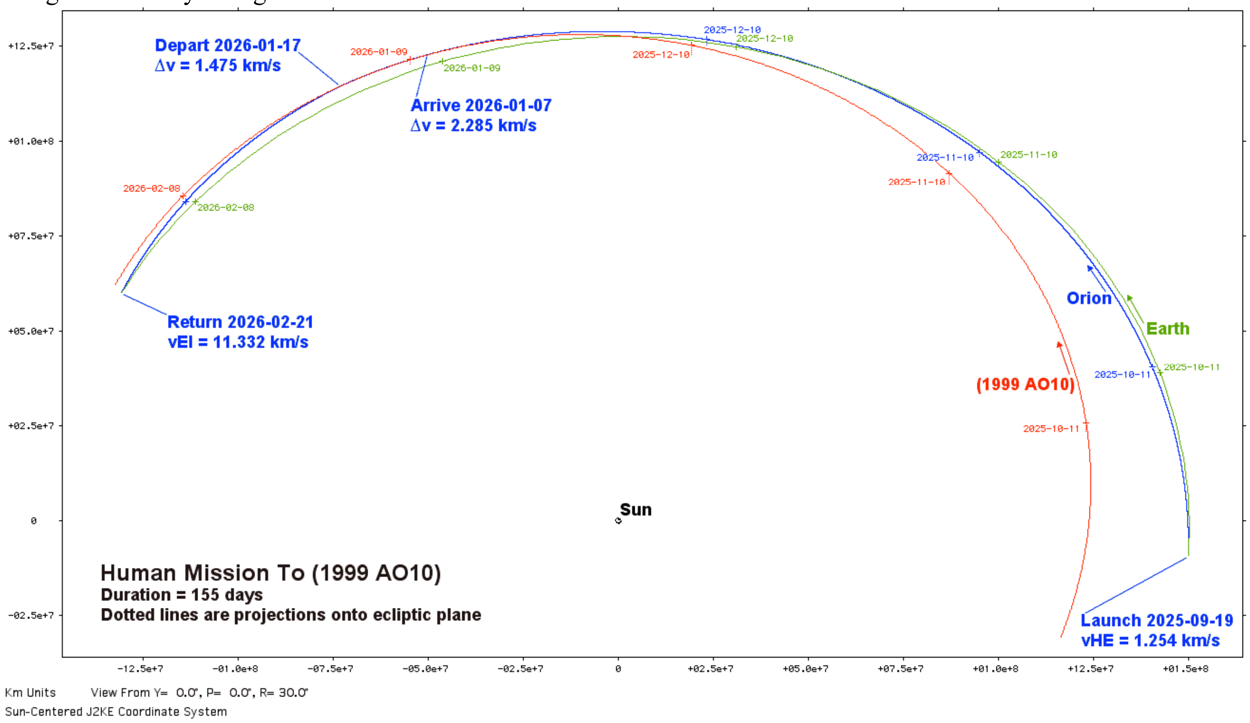

Figure 6: Heliocentric (1999 AO_{10}) Human Mission Trajectory

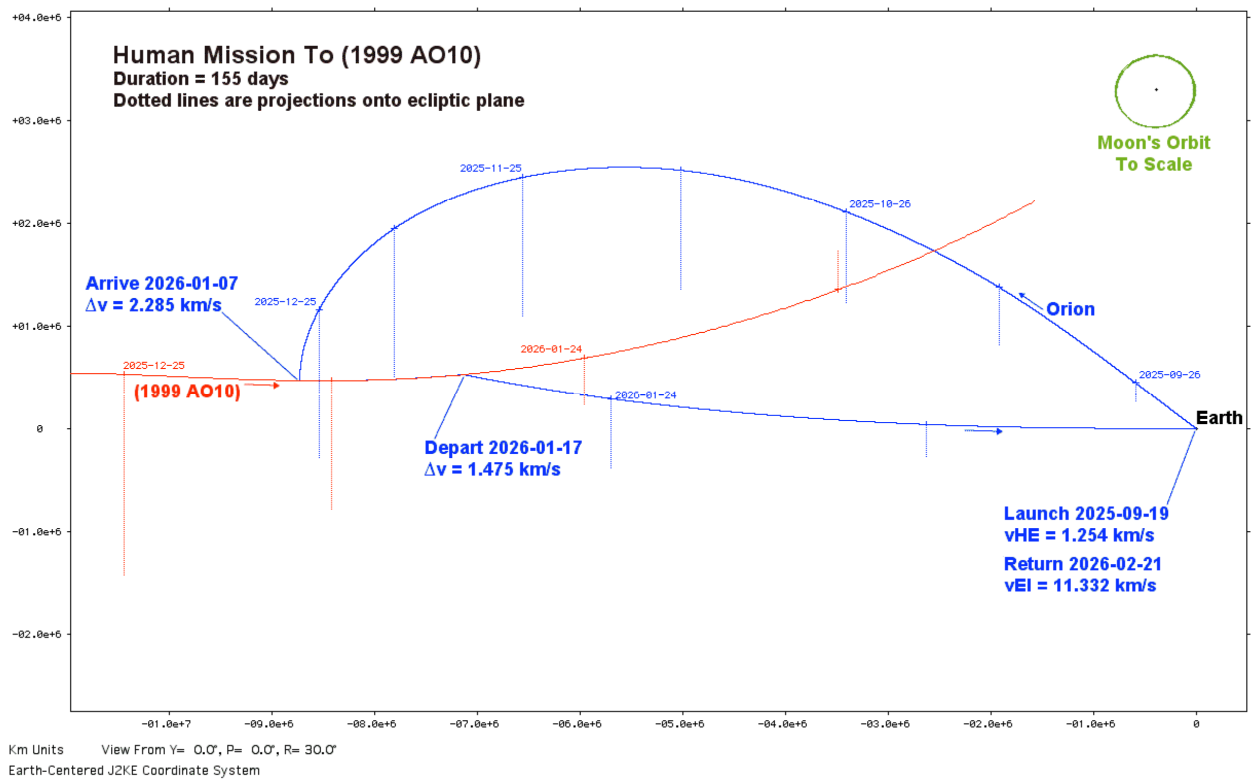

Figure 7: Geocentric (1999 AO_{10}) Human Mission Trajectory

Stage #3 mission assessments akin to the foregoing (1999 AO_{10}) example have been performed for additional Table 3 Earth encounters with the Accessible 36 NEO destinations. Results from these notional trajectory designs are summarized in Table 5.

Table 5: Summary Of Notionally Optimized Mission Designs Associated With Some Table 3 Encounters

Enc. #	Designation	~Diam. (m)	Launch Date	v_{HE} (km/s)	Δv_A (km/s)	Δv_D (km/s)	v_{EI} (km/s)	ΔT (days)
1	(1996 XB_{27})	150	2027 Jan 31	4.327	3.937	3.514	11.230	260
2	(1996 XB_{27})	150	2049 Jan 01	2.586	3.693	3.331	11.431	290
3	(1998 HG_{49})	143	2031 Apr 21	2.504	3.712	3.200	11.847	240
5	(2001 BB_{16})	104	2034 Nov 30	2.425	1.964	2.871	11.227	240
7	(2003 SM_{84})	99	2040 Feb 20	1.383	2.780	1.051	11.236	210
8	(2003 SM_{84})	99	2046 Mar 22	1.467	2.054	1.378	11.177	180
9	(2000 AE_{205})	90	2048 Jun 11	2.868	2.796	2.750	11.262	220
10	(2001 QJ_{142})	72	2024 Apr 10	2.115	1.102	2.386	11.352	200
11	(1999 AO_{10})	57	2025 Sep 19	1.254	2.285	1.475	11.332	155
13	(2008 BT_2)	47	2021 Dec 12	1.569	2.921	3.104	11.425	270
14	(2008 CX_{118})	45	2024 Jan 11	2.164	2.551	2.273	11.162	350
16	(2001 FR_{85})	43	2039 Aug 30	1.642	2.094	0.847	11.513	210
19	(2000 SG_{344})	38	2028 Feb 09	0.298	0.754	1.754	11.124	310
23	(1999 CG_9)	31	2033 Dec 30	1.867	2.290	2.296	11.355	220
24	(2005 ER_{95})	30	2027 Dec 11	0.749	3.459	2.666	11.107	260
25	(2006 BZ_{147})	29	2035 Jan 29	2.553	0.919	1.060	11.572	360
36	(2001 GP_2)	14	2019 Dec 09	1.522	2.073	0.170	11.339	304
39	(2008 EA_9)	10	2019 Nov 30	2.186	0.979	1.762	11.214	155
47	(2007 UN_{12})	6	2020 Jul 18	2.679	1.109	1.707	11.346	190
53	(2006 RH_{120})	4	2028 Mar 31	0.901	2.042	1.606	11.224	130

The sum $\Delta v_A + \Delta v_D$ for each of the 20 Table 5 missions is plotted against the associated NEO/Earth encounter's r_{MIN} from Table 3 in Figure 8. A correlation between these two variables is evident such that all Figure 8 points fall above the dotted line $\Delta v_A + \Delta v_D$ [km/s] = 25 r_{MIN} [AU][§§§]. With the Stage #1 filter's Assumption B equating to $\Delta v_A + \Delta v_D < 3$ km/s, Figure 8's correlation would impose a Stage #2 encounter search constraint of $r_{MIN} < 3/25 = 0.12$ AU. This criterion is in close agreement with the encounter search strategy documented in Section IV. At a more optimistic capability equivalent to $\Delta v_A + \Delta v_D < 5$ km/s, Stage #2 searches constrained to $r_{MIN} < 5/25 = 0.2$ AU would be appropriate. Because Stage #2 encounter searches with $r_{MIN} > 0.1$ AU were only performed for (1996 XB_{27}) and (1998 HG_{49}), the two largest members of the Accessible 36, other Figure 8 points for missions to smaller Accessible 36 destinations undoubtedly exist for $r_{MIN} > 0.1$ AU. It remains to be verified where these points fall with respect to the "$\Delta v_A + \Delta v_D$ [km/s] = 25 r_{MIN} [AU]" line. Finally, note how the lone mission opportunity to marginally inaccessible (1998 HG_{49}) becomes an outlying point in Figure 8. Although this mission's $\Delta v_A + \Delta v_D$ is competitive with those pertaining to the two (1996 XB_{27}) missions, its v_{EI} is more than 0.4 km/s greater than that of either (1996 XB_{27}) mission and is the largest such value in Table 5.

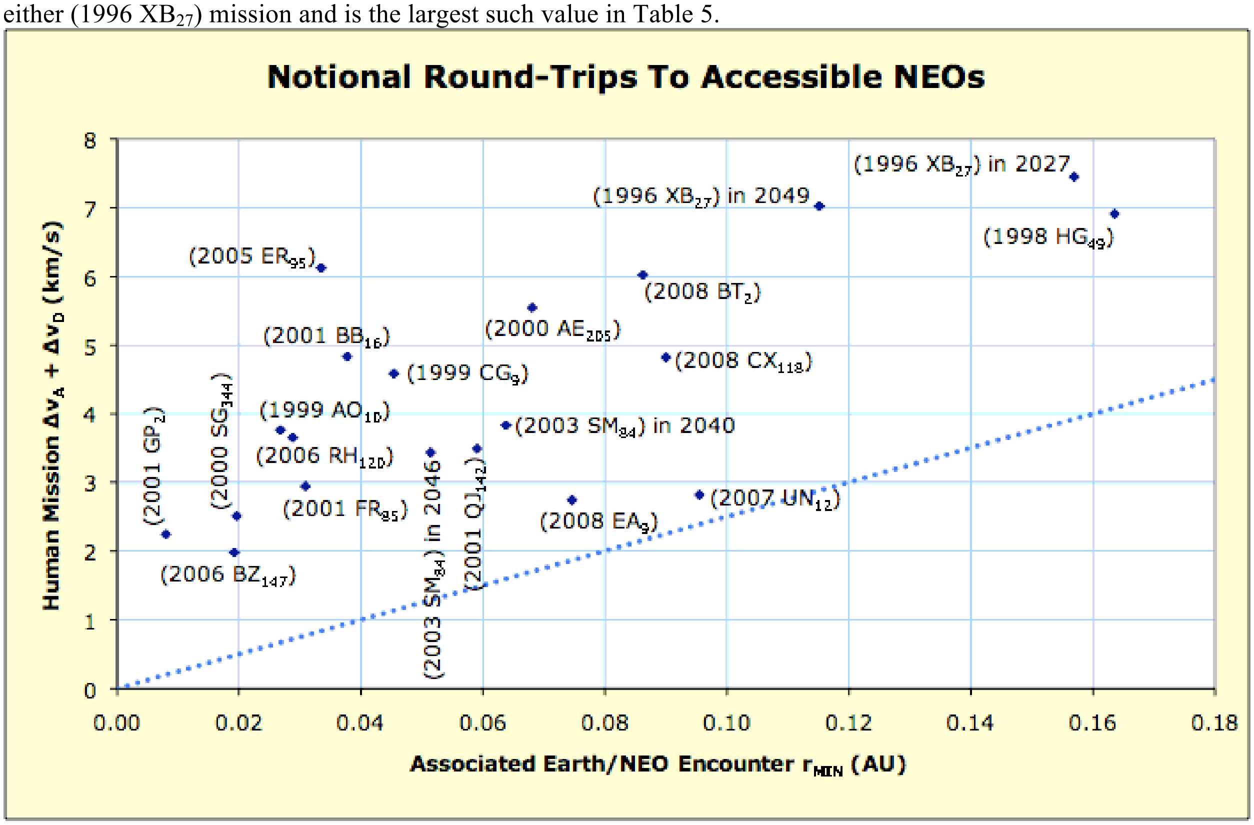

Figure 8: Correlation Between $\Delta v_A + \Delta v_D$ And NEO/Earth Encounter r_{MIN} In Table 5 Missions

VI. Conclusion

A 3-stage survey process to identify and assess human NEO mission prospects has been documented and applied to JPL's current SBDB in the context of anticipated beyond-LEO human exploration capabilities. No less than 36

[§§§] The 25 km/s/AU slope in this relationship is reasonably in accord with constant speed transits covering r_{MIN} in 6 months. For example, consider r_{MIN} = 0.04 AU = 5,983,915 km. Covering this distance in 6 months = 182 days = 15,724,800 s requires a constant speed of 0.381 km/s, approximating Δv_A or Δv_D in this simplified model. When doubled to approximate $\Delta v_A + \Delta v_D$, in Figure 8, constant speed change at the NEO is 0.761 km/s. The constant speed equivalent slope from this example is then 0.761/0.04 = 19.0 km/s/AU. The dotted line passing through the Figure 8 origin with 25 km/s/AU slope should therefore pass below all real world mission design points excepting those of nearly one-year duration whose NEO destinations have nearly zero geocentric relative motion at spacecraft arrival and departure.

potentially accessible human mission destinations were culled from the SBDB in June 2009. Over the interval from 2020 to 2050, these destinations give rise to at least 58 potential mission opportunities coinciding with NEO/Earth encounters closer than ~0.1 AU. Of these opportunities, half a dozen require storable propulsive capability at the NEO destination less than the 3 km/s change-in-velocity assumed as an initial accessibility criterion. If this capability is augmented, viable mission opportunities proliferate dramatically. As the SBDB is populated with an order of magnitude more NEOs in the coming decades, opportunities using any exploration capability appreciably beyond that achieved during the Apollo Program will increase unconditionally. To illustrate this population explosion, Stage #1's filter again polled the SBDB in November 2009. From discoveries catalogued in the 5 months since June, (2009 OS_5) and (2009 RT_1) have joined the Accessible 36 as potential human exploration destinations,

Acknowledgments

The authors wish to acknowledge two significant technical contributors to the SBDB survey of accessible human exploration destinations. NASA-MSFC/J. Phil Sumrall supplemented Figure 1 with detailed pedigree information on Ares V performance data communicated in a timely fashion. JPL/Ted H. Sweetser reviewed the Stage #1 filter in detail, helping identify and correct a critical error. These contributions are examples of the unified "One NASA" culture whose cooperative teamwork will lead to human exploration far beyond LEO.

References

[1] Review of U.S. Human Spaceflight Plans Committee, *Seeking a Human Spaceflight Program Worthy of a Great Nation*, NASA, October 2009, http://www.nasa.gov/pdf/396093main_HSF_Cmte_FinalReport.pdf [retrieved 28 October 2009].

[2] Landis, R. R., Abell, P. A., Korsmeyer, D. J., Jones, T. D., and Adamo, D. R., “Piloted operations at a near-Earth object (NEO)”, *Acta Astronautica*, Vol. 65, Elsevier, Amsterdam, The Netherlands, pp. 1689-1697, 2009.

[3] Wikipedia contributors, "Apollo Command/Service Module", *Wikipedia, The Free Encyclopedia,* http://en.wikipedia.org/wiki/Apollo_Command_Module#References [retrieved 29 October 2009].

[4] NASA, "NASA's Exploration Systems Architecture Study Final Report", NASA-TM-2005-214062, November 2005, www.nasa.gov/directorates/esmd/news/ESAS_report.html [retrieved 28 October 2009].

[5] Brown, C. D., *Spacecraft Mission Design*, AIAA Education Series, Washington, D.C., 1992.

[6] Sumrall, J. P., "Ares V Overview", Ares V Solar System Science Workshop, 16 April 2008.

[7] Giorgini, J. D., Yeomans, D. K., Chamberlin, A. B., Chodas, P. W., Jacobson, R. A., Keesey, M. S., Lieske, J. H., Ostro, S. J., Standish, E. M., Wimberly, R. N., "JPL's On-Line Solar System Data Service", *Bulletin of the American Astronomical Society*, Vol. 28, No. 3, 1996, p. 1158.

[8] Yeomans, D. K., personal communication, 12 June 2009.

[9] Meeus, J., *Astronomical Algorithms*, Willmann-Bell, Inc., Richmond, VA, 1991, Appendix II.

[10] Orloff, R. W. and Harland, D. M., *Apollo: The Definitive Sourcebook*, Springer-Praxis Books In Space Exploration, New York City, NY, 2006.